

# MHD turbulence sheared in fixed and rotating frames

By S. C. Kassinos<sup>†</sup>, B. Knaepen<sup>‡</sup> AND A. Wray

We consider homogeneous turbulence in a conducting fluid that is exposed to a uniform external magnetic field while being sheared in fixed and rotating frames. We take both the frame-rotation axis and the applied magnetic field to be aligned in the direction normal to the plane of the mean shear. Here a systematic parametric study is carried out in a series of Direct Numerical Simulations (DNS) in order to clarify the main effects determining the structural anisotropy and stability of the flow. When the time scale of the mean shear is short compared to the Joule time ( $\tau_{\text{shear}} \ll \tau_m$ ), we find that the turbulence structures tend to align preferentially with the streamwise direction irrespective of the magnetic Reynolds number,  $R_m$ . When  $\tau_{\text{shear}} \gg \tau_m$ , we find that at low  $R_m$  the turbulent eddies become elongated and aligned with the magnetic field, but at moderately high  $R_m$ , there is partial streamwise alignment of the eddies. When  $\tau_{\text{shear}} \approx \tau_m$ , we find that competing mechanisms tend to produce different structural anisotropies and small variations in dimensionless parameters can have a strong effect on the structure of the evolving flow. For example, for very low  $R_m$ , a preferential alignment of structures in the direction of the magnetic field emerges as the flow evolves, consistent with the predictions of the quasi-static approach. For  $R_m \sim 1$ , the structures are found to be equally aligned in the streamwise and spanwise direction at large times. However, when  $R_m$  is moderately high ( $10 \lesssim R_m \lesssim 50$ ) this strong spanwise alignment is replaced by a preferential alignment of structures in the streamwise direction. Counter to intuition, we found evidence that strong rotation in combination with a spanwise magnetic field tends to promote a streamwise alignment of the eddies, at least when  $\tau_{\text{shear}} \approx \tau_m$ . In some cases with frame counter-rotation, we have observed a bifurcation that leads to 2D turbulence consisting of vertical slabs parallel to the plane of the mean shear. For sufficiently high magnetic Reynolds numbers ( $R_m \sim 50$ ) and strong frame counter-rotation, we find that the magnetic energy exceeds the turbulent kinetic energy. In this regime the ratio of production to dissipation exceeds unity ( $P/\epsilon > 1$ ) even when the ratio of the frame rotation rate to the shear rate is such that that in the hydrodynamic case suppression of the turbulence ( $P/\epsilon < 1$ ) is observed. Finally, we also examine the range of validity of the Quasi-Linear approximation by comparing its predictions to those of ideal MHD. The QL approximation is found to be in excellent agreement with full MHD for the entire range of magnetic Reynolds numbers ( $R_m$ ) that was examined ( $R_m \leq 50$ ).

---

## 1. Introduction

### 1.1. Motivation and objectives

The combined effects of mean shear, frame rotation and an externally-applied magnetic field on turbulence in a conducting fluid are relevant to the accretion of Keplerian disks,

<sup>†</sup> Mechanical and Manufacturing Engineering, University of Cyprus and CTR NASA/Ames

<sup>‡</sup> Université Libre de Bruxelles, Belgium and CTR NASA/Ames

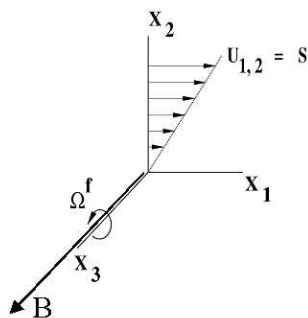


FIGURE 1. Configuration for shear in a rotating frame. Here  $B$  denotes the external magnetic field (when applicable),  $\Omega^f$  the frame rotation rate, and  $S$  the shear rate.

to magnetic stirring, fusion plasma, and to Magnetogasdynamic (MGD) applications, involving advanced flow-control and propulsion schemes for hypersonic vehicles.

CFD codes used for the prediction of MHD and MGD flows rely on simple turbulence models, like  $k$ - $\epsilon$  models, with additional *ad hoc* modifications to account for the effects of the magnetic field. Such closures neglect the important dynamical role that the structure of the turbulence plays in the interaction between the turbulence and the applied magnetic field. As a result, they tend to be of limited applicability.

Structure-Based Models (SBM) are by construction able to account for the dynamical effects of the energy-containing turbulence structure. Preliminary work in the case of homogeneous unstrained MHD turbulence (Kassinos & Reynolds 1999), has shown that SBM are well suited for use in the prediction of MHD and MGD applications. The task of developing turbulence SBM or other closures for MHD and MGD applications can be simplified by taking advantage of approximations to the governing equations that are valid in flow regimes typically encountered in technological applications. In order to proceed further towards the development of SBM for MHD turbulence it is important to understand the combined effects of mean shear and frame rotation on MHD turbulence.

In the purely hydrodynamic case, frame rotation can act to either stabilize or destabilize homogeneous shear flow. For example, in these flows the equilibrium state depends on the ratio of the frame rotation rate  $\Omega^f \equiv \Omega_{12}^f$  to the shear rate  $S \equiv U_{1,2}$  (see Fig. 1). A limited range of values of  $\lambda = \Omega^f/S$  is marked by exponential growth of both the turbulent kinetic energy,  $k$ , and the dissipation rate,  $\epsilon$ . This has been known for a while, but details of the equilibrium state of the turbulence, such as the behavior of the ratio of the turbulent kinetic energy production and dissipation rates,  $P/\epsilon$ , remained unclear. Virtually all algebraic stress and Reynolds stress transport models using the standard  $\epsilon$  equation predict that, within this range, equilibrium turbulence is marked by  $P/\epsilon$  being constant and independent of  $\lambda$ . This behavior has been reported in the literature and, in the absence of DNS data that would have helped evaluate it, has been accepted as reflecting the correct physics. Preliminary results from a DNS by Kassinos, Reynolds, and Wray (see for example Kassinos & Reynolds (2003)) show that in fact the equilibrium value of  $P/\epsilon$  is a function of  $\lambda$ , as shown in Figure 2. When  $\lambda = \Omega^f/S$  is close to  $1/4$  the turbulent kinetic energy grows exponentially, and the energy-containing structures tend to quickly fill the computational box and the simulation has to be terminated. Thus obtaining reliable equilibrium values for  $P/\epsilon$  when  $\lambda = \Omega^f/S \sim 1/4$  is challenging. However, in the neighborhood of  $\lambda \approx 0.55$ , the structures grow relatively slowly and

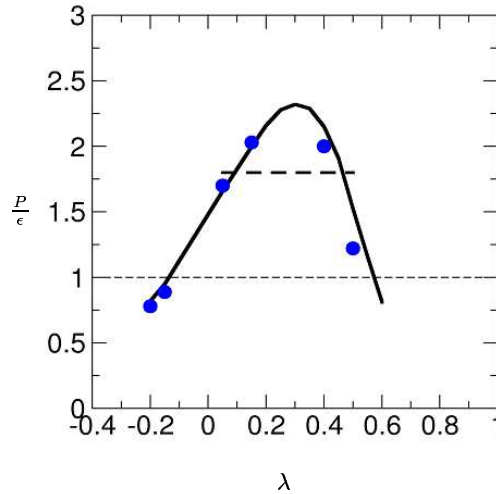


FIGURE 2. The variation of the ratio of production to dissipation ( $P/\epsilon$ ) of the turbulent kinetic energy with the ratio of frame rotation to shear rate  $\eta$ . Positive values of  $\lambda$  correspond to a frame counter-rotating relative to the intrinsic shear rotation sense:  $\bullet$ , DNS (Kassinis & Reynolds, 2002); — Structure-based model; ---- model using standard

they are well contained within the computational box as equilibrium is approached. For this reason, it is clear from these simulations that the turbulence is suppressed when the frame counter-rotates at a rate of  $\lambda \approx 0.55$  or higher.

For vanishingly small magnetic Reynolds numbers ( $R_m \ll 1$ ), the induced magnetic fluctuations are much weaker than the applied field and their characteristic time scale, based on their diffusion, is much shorter than the eddy turnover time. A classical approximation for decaying MHD turbulence at low  $R_m$  is the Quasi-Static (QS) approximation. In this approximation, the induced magnetic field fluctuations become a linear function of the velocity field. Kassinis, Knaepen & Carati (2002) and Knaepen, Kassinis & Carati (2004) considered the case of initially isotropic decaying MHD turbulence, and concluded that the QS approximation was reasonably accurate for  $R_m \lesssim 1$ . For higher  $R_m$ , where the QS approximation fails, they proposed the use of the Quasi-Linear (QL) approximation, which amounts to retaining the unsteady term in the magnetic induction equation, retaining the non-linear hydrodynamic terms in the fluctuating momentum equation, but dropping all the nonlinear terms involving the magnetic fluctuations. They carried out a series of DNS and concluded that in unstrained MHD turbulence the QL approximation was valid for the entire range of magnetic Reynolds numbers they examined ( $R_m \lesssim 30$ ).

Surprisingly, little work has been done to explore the structure of homogeneous MHD turbulence under the influence of mean shear and frame rotation. The objective of this work is to use DNS to probe the fundamental physics in sheared MHD turbulence. Primarily, we are interested in understanding the effects of shear and rotation on the dynamics of MHD turbulence, including the structural morphology and stability of these flows. For example, it is important to establish how the bifurcation diagram of Fig. 2 is modified in the MHD case. Stability modifications due to the presence of the magnetic field can potentially have implications for the evolution of stellar accretion disks and is an important element that must be built into a successful model for MHD turbulence.

We start by discussing the relevant dimensionless parameters that characterize MHD

and MGD flows in the presence of mean shear and frame rotation. In section 3 we introduce the governing equations for ideal MHD and the simplifications associated with the QL approximation as introduced by Kassinos *et al.* (2002) and Kneapen *et al.* (2004). The numerical code and associated initial conditions are described in section 4, while section 5 is devoted to a discussion of the most important results. A concluding summary is given in section 6.

## 2. Dimensionless parameters

The effects of a uniform magnetic field applied to unstrained homogeneous turbulence in an electrically conductive fluid are characterized by three dimensionless parameters. The first of these is the magnetic Reynolds number

$$R_m = \frac{vL}{\eta} = \left(\frac{v}{L}\right)\left(\frac{L^2}{\eta}\right), \quad (2.1)$$

where  $L$  is the integral length scale and  $v$  is the r.m.s. fluctuating velocity

$$v = \sqrt{R_{ii}/3}, \quad R_{ij} = \overline{u_i u_j}. \quad (2.2)$$

Here  $u_i$  is the fluctuating velocity, and  $\eta$  is the magnetic diffusivity

$$\eta = 1/(\sigma\mu^*) \quad (2.3)$$

where  $\sigma$  is the electric conductivity of the fluid, and  $\mu^*$  is the fluid magnetic permeability (here we use  $\mu^*$  for the magnetic permeability and reserve  $\mu$  for the dynamic viscosity). Thus the magnetic Reynolds number represents the ratio of the characteristic time scale for diffusion of the magnetic field to the time scale of the turbulence. In the case of vanishingly small  $R_m$ , the distortion of the magnetic field lines by the fluid turbulence is sufficiently small that the induced magnetic fluctuations  $\mathbf{b}$  around the mean (imposed) magnetic field  $\mathbf{B}$  are also small.

The second parameter is the magnetic Prandtl number representing the ratio of  $R_m$  to the hydrodynamic Reynolds number  $Re_L$

$$P_m \equiv \frac{\nu}{\eta} = \frac{R_m}{Re_L}, \quad Re_L = \frac{vL}{\nu}. \quad (2.4)$$

The magnetic-interaction number (or Stuart number) is

$$N \equiv \frac{\sigma B^2 L}{\rho v} = \frac{(B^{\text{ext}})^2 L}{\eta} \frac{L}{v} = \frac{\tau}{\tau_m}, \quad (2.5)$$

where  $B$  is the magnitude of the magnetic field,  $B^{\text{ext}} = B/\sqrt{\mu^*\rho}$  is the magnetic field expressed in Alfvén units, and  $\rho$  is the fluid density.  $N$  represents the ratio of the large-eddy turnover time  $\tau$  to the Joule time  $\tau_m$ , i.e. the characteristic time scale for dissipation of turbulent kinetic energy by the action of the Lorentz force.  $N$  parametrizes the ability of an imposed magnetic field to drive the turbulence to a two-dimensional three-component state. In the absence of mean shear and frame rotation, the continuous action of the Lorentz force tends to concentrate energy in modes independent of the coordinate direction aligned with  $\mathbf{B}$ . As a two-dimensional state is approached, Joule dissipation decreases because fewer and fewer modes with gradients in the direction of  $\mathbf{B}$  are left available.

In addition, the tendency towards two-dimensionality and anisotropy is continuously opposed by non-linear angular energy transfer from modes perpendicular to  $\mathbf{B}$  to other modes, which tends to restore isotropy. If  $N$  is larger than some critical value  $N_c$ , the Lorentz force is able to drive the turbulence to a state of complete two-dimensionality. For smaller  $N$ , the Joule dissipation is balanced by non-linear transfer before a complete two-dimensionality is reached. For very small  $N$  ( $N \leq 1$ ), the anisotropy induced by the Joule dissipation is negligible. Here we consider  $N$  in the range 1 – 20.

In the presence of mean shear and frame rotation, two additional parameters become important. The first of these is the ratio of the time scale of the mean shear to the Joule time  $\tau_m$ ,

$$M \equiv \frac{(B^{\text{ext}})^2}{\eta S} = \frac{\tau_{\text{shear}}}{\tau_m} \quad (2.6)$$

where  $S$  is the mean shear rate. The second is the ratio of the frame rotation rate  $\Omega^f$  to shear rate  $S$ ,

$$\lambda \equiv \frac{\Omega^f}{S} \quad (2.7)$$

where  $\Omega^f = -\Omega_{12}^f$  so that positive values of  $\lambda$  correspond to a frame counter-rotating relative to the sense of rotation associated with the mean shear.

### 3. Governing Equations

Transport in homogeneous MHD shear flow is described by the incompressible MHD equations

$$\tilde{u}_{i,i} = 0 \quad \tilde{b}_{i,i} = 0 \quad (3.1)$$

$$\partial_t \tilde{u}_i + \tilde{u}_s \tilde{u}_{i,s} = -\frac{1}{\rho} P_{,i}^* + \tilde{b}_{i,m} \tilde{b}_m + \nu \tilde{u}_{i,ss} \quad (3.2)$$

$$\partial_t \tilde{b}_i + \tilde{u}_s \tilde{b}_{i,s} = \tilde{b}_s \tilde{u}_{i,s} + \eta \tilde{b}_{i,ss} \quad (3.3)$$

where  $P^*$  is the total pressure including magnetic contributions,  $\tilde{b}_i$  is the magnetic field in Alfvén units, and  $\tilde{u}_i$  are the velocity components. Next, the flow variables are transformed into a rotating frame, where they are explicitly decomposed into a mean and a fluctuating part. We solve the resulting governing equations for the fluctuation fields in a coordinate system that deforms with the mean flow so that Fourier decomposition methods can be employed. In this deforming coordinate system, the transformed equations become

$$\begin{aligned} \partial_t v_i + G_{ik} v_k + \frac{\partial v_i}{\partial x_m} v_k A_{mk} + 2\Omega_{ik}^f v_k = -\frac{1}{\rho} \frac{\partial p}{\partial x_m} A_{mi} \\ + \frac{\partial B_i^{\text{ext}}}{\partial x_m} b_k A_{mk} + \frac{\partial b_i}{\partial x_m} B_k^{\text{ext}} A_{mk} + \frac{\partial b_i}{\partial x_m} b_k A_{mk} + \nu \frac{\partial^2 v_i}{\partial x_k \partial x_z} A_{zp} A_{kp} \end{aligned} \quad (3.4)$$

and

$$\begin{aligned} \partial_t b_i - G_{ik} b_k &= -v_k \frac{\partial B_i^{\text{ext}}}{\partial x_m} A_{mk} - v_k \frac{\partial b_i}{\partial x_m} A_{mk} \\ &+ B_k^{\text{ext}} \frac{\partial v_i}{\partial x_m} A_{mk} + b_k \frac{\partial v_i}{\partial x_m} A_{mk} + \eta \frac{\partial^2 b_i}{\partial x_k \partial x_z} A_{zp} A_{kp}. \end{aligned} \quad (3.5)$$

Here,  $v_i$  and  $b_i$  are the components of velocity and magnetic fluctuation fields transformed in the rotating frame,  $x_i$  are deforming coordinates,  $G_{ij} = U_{i,j}$  is the mean velocity gradient tensor, and  $A_{ij}$  is the (Rogallo) transformation matrix satisfying

$$\dot{A}_{iz} + A_{ij} G_{jz} = 0. \quad (3.6)$$

In the hydrodynamic case, one can impose any mean strain tensor, but once the mean strain is specified, the homogeneity requirement imposes constraints on the evolution of the mean rotation tensor. In the MHD case, these constraints involve gradients of the mean magnetic field as well. However, when the frame rotation axis and the uniform mean magnetic field vector are perpendicular to the plane of shear, these constraints leave the mean rotation unmodified and need not be considered.

### 3.1. The Quasi-Linear (QL) approximation

The Quasi-Linear (QL) approximation was introduced by Kassinis, Knaepen & Carati (2002) and Knaepen, Kassinis & Carati (2004) as a moderate- $R_m$  replacement to the classical Quasi-Static approximation Roberts (1967). The QL approximation amounts to neglecting the nonlinear terms involving the fluctuating magnetic field in (3.4) and (3.5),

$$\begin{aligned} \partial_t v_i + G_{ik} v_k + \frac{\partial v_i}{\partial x_m} v_k A_{mk} + 2\Omega_{ik}^f v_k &= -\frac{1}{\rho} \frac{\partial p}{\partial x_m} A_{mi} \\ &+ \frac{\partial B_i^{\text{ext}}}{\partial x_m} b_k A_{mk} + \frac{\partial b_i}{\partial x_m} B_k^{\text{ext}} A_{mk} + \nu \frac{\partial^2 v_i}{\partial x_k \partial x_z} A_{zp} A_{kp} \end{aligned} \quad (3.7)$$

and

$$\partial_t b_i - G_{ik} b_k = -v_k \frac{\partial B_i^{\text{ext}}}{\partial x_m} A_{mk} + B_k^{\text{ext}} \frac{\partial v_i}{\partial x_m} A_{mk} + \eta \frac{\partial^2 b_i}{\partial x_k \partial x_z} A_{zp} A_{kp}. \quad (3.8)$$

Note that the nonlinear convective term in the fluctuating momentum equation and the unsteady term  $\partial_t b_i$  in the fluctuating induction equation are both retained. Of course, if the later is also neglected one recovers the QS approximation.

## 4. Numerical code and initial conditions

We have used a pseudo-spectral code with the ability to simulate either the full MHD equations (3.4) and (3.5), or the reduced QL equations (3.7) and (3.8). The numerical method used to solve the governing equations for homogeneous shear flows is similar to that introduced by Rogallo (1981). The governing equations are transformed to a set of coordinates which deform with the mean flow. This allows Fourier pseudo-spectral methods, with periodic boundary conditions, to be used for the representation of the spatial variation of the flow variables. Time advance is accomplished by a third-order Runge-Kutta method. Since the mean imposed shear skews the computational grid with time, periodic remeshing of the grid is needed in order to allow the simulation to progress to large total shear, where a self-preserving regime might be expected to prevail. The periodic remeshing introduces aliasing errors that are removed by a de-aliasing procedure

---

Resolution	256 <sup>3</sup>
Box size ( $\ell_x \times \ell_y \times \ell_z$ )	$2\pi \times 2\pi \times 2\pi$
Rms velocity ( $v$ )	3.099
Viscosity	0.006
Integral length-scale ( $3\pi/4 \times (\int k^{-1} E(k) dk / \int E(k) dk)$ )	0.322
$Re = uL/v$	166
Dissipation ( $\epsilon$ )	47.876
Dissipation scale ( $\gamma = (\nu^3/\epsilon)^{(1/4)}$ )	0.0082
$k_{\max}\gamma$	1.82
Microscale Reynolds number ( $Re_\lambda = \sqrt{15/(\nu\epsilon)}u^2$ )	69.40
Eddy turnover time ( $\tau = (3/2)u/\epsilon$ )	0.097

---

TABLE 1. Turbulence characteristics of the initial velocity field. All quantities are in MKS units.

---

included in the code. An MPI based version of the code has been implemented in the Vectoral language and tested individually for accuracy, grid independence, and scalability.

All the runs presented here have a resolution of 256<sup>3</sup> Fourier modes in a  $(2\pi)^3$  computational domain. The initial conditions for the velocity were common to all cases. They were created starting with a pulse of energy at low wave numbers in Fourier space and a random distribution of phases for the Fourier modes. In order to let the higher-order statistics develop, the flow was evolved in the absence of mean shear or frame rotation and without a mean magnetic field, while forcing was being applied to the low wave number region of the spectrum. This initial phase was continued until an equilibrium state was reached and the skewness acquired its peak value. At that time, hereafter referred to as  $t_0$ , the external magnetic field, mean shear and frame rotation were switched on while the artificial forcing was eliminated. The characteristics of the initial field at time  $t_0$  are summarized in Table 1.

In the MHD runs, an initial condition for  $b_i$  has to be chosen at  $t = t_0$ . Here we have made the choice  $b_i(t_0) = 0$ . In other words, our simulations describe the response of an initially non-magnetized turbulent conductive fluid to the application of a mean magnetic field. The corresponding completely-linearized problem in the absence of mean shear and frame rotation has been described in detail in Moffatt (1967).

#### 4.1. Parameters

In order to distinguish between our numerical runs, we will vary the magnetic Reynolds number  $R_m$ , the magnetic interaction number  $N$ , the ratio of the timescale of the mean shear to that for magnetic diffusion  $M$ , and the ratio of the frame rotation rate to the mean shear rate  $\lambda$ . Specification of  $R_m$  and  $N$  completely determines  $\eta$  and  $B^{\text{ext}}$  according to:

$$B^{\text{ext}} = \frac{Nv^2}{R_m}, \quad \eta = \frac{vL}{R_m}. \quad (4.1)$$

The values of these parameters for the different runs considered are summarized in Table 2. The entries in Table 2 are grouped first according to the initial value of  $M$ , then according to the value of the Magnetic Stuart number  $N$ , and last according to the magnetic Reynolds number  $R_m$ . Thus, the identification number of run CX.Y.Z can be

#	Case	$\eta$	$B^{ext}$	$N(t_0)$	$R_m(t_0)$	$M$	$\lambda$
1	C1.1.1	207.75	3.11	1	0.1	0.1	0.0, 0.25
2	C1.1.5	.387	.696	1	2.0	0.1	0.0, 0.25
3	C1.1.10	.258	.568	1	3.0	0.1	0.0, 0.25
4	C1.1.20	.155	.440	1	5.0	0.1	0.0, 0.25
5	C1.1.50	.0775	.311	1	10.0	0.1	0.0, 0.25
6	C1.2.1	7.75	9.84	10	0.1	0.1	0.0, 0.25
7	C1.2.5	.387	2.20	10	2.0	0.1	0.0, 0.25
8	C1.2.10	.258	1.80	10	3.0	0.1	0.0, 0.25
9	C1.2.20	.155	1.39	10	5.0	0.1	0.0, 0.25
10	C1.2.50	.0775	.984	10	10.0	0.1	0.0, 0.25
11	C2.1.1	7.75	22.0	50	0.1	2	0.0,0.25,0.5,0.75,1.0
12	C2.1.5	.387	4.92	50	2.0	2	0.0,0.25,0.5,0.75,1.0
13	C2.1.10	.258	4.02	50	3.0	2	0.0,0.25,0.5,0.75,1.0
14	C2.1.20	.155	3.11	50	5.0	2	0.0,0.25,0.5,0.75,1.0
15	C2.1.50	.0775	2.20	50	10.0	2	0.0,0.25,0.5,0.75,1.0
16	C2.2.1	7.75	22.0	50	0.1	2	0.0,0.25,0.5,0.75,1.0
17	C2.2.5	.387	4.92	50	2.0	2	0.0,0.25,0.5,0.75,1.0
18	C2.2.10	.258	4.02	50	3.0	2	0.0,0.25,0.5,0.75,1.0
19	C2.2.20	.155	3.11	50	5.0	2	0.0,0.25,0.5,0.75,1.0
20	C2.2.50	.0775	2.20	50	10.0	2	0.0,0.25,0.5,0.75,1.0
21	C3.1.1	7.75	22.0	50	0.1	20	0.0,0.25
22	C3.1.5	.387	4.92	50	2.0	20	0.0,0.25
23	C3.1.10	.258	4.02	50	3.0	20	0.0,0.25
24	C3.1.20	.155	3.11	50	5.0	20	0.0,0.25
25	C3.1.50	.0775	2.20	50	10.0	20	0.0,0.25
26	C3.2.1	7.75	22.0	50	0.1	20	0.0,0.25
27	C3.2.5	.387	4.92	50	2.0	20	0.0,0.25
28	C3.2.10	.258	4.02	50	3.0	20	0.0,0.25
29	C3.2.20	.155	3.11	50	5.0	20	0.0,0.25
30	C3.2.50	.0775	2.20	50	10.0	20	0.0,0.25

TABLE 2. Summary of the parameters for the different runs performed

interpreted as follows:

$$\begin{aligned}
X = 1 &\Rightarrow M(t_0) = 0.1 & X = 2 &\Rightarrow M(t_0) = 2 & X = 3 &\Rightarrow M(t_0) = 20 \\
Y = 1 &\Rightarrow N(t_0) = 1 & Y = 2 &\Rightarrow N(t_0) = 10
\end{aligned}
\tag{4.2}$$

and where  $Z$  is such that  $R_m = Z$ . Thus, for the first ten runs we have  $M = 0.1$ ; for the next ten  $M = 2$  and finally, for runs 21-30 we have  $M = 20$ .

## 5. Results

In this section we discuss some of the more important results obtained by carrying out the simulations described in the previous sections.

### 5.1. Eddy alignment

The effects of mean shear, frame rotation, and external magnetic fields on the turbulence structure are well understood whenever these act independently. Mean shear tends to

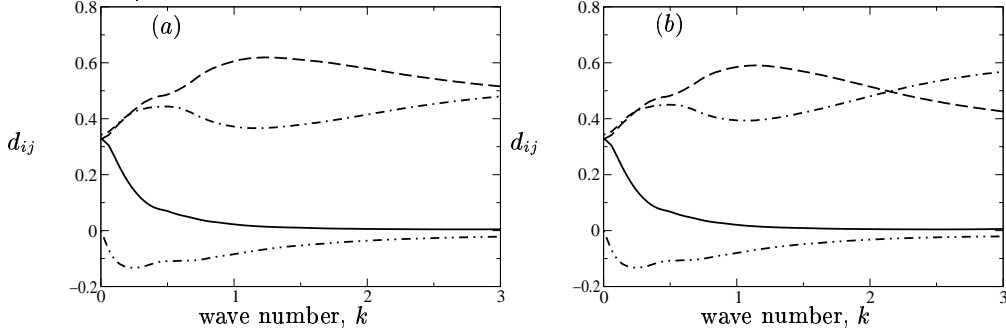


FIGURE 3. Structure anisotropy as measured by  $d_{ij}$  (see 5.1) in homogeneous MHD turbulence being sheared in a fixed frame ( $\lambda = 0$ ) for the case with  $M = \tau_{\text{shear}}/\tau_m = 0.1$ : —  $d_{11}$ ; ---  $d_{22}$ ; -·-·-  $d_{33}$ ; ····  $d_{12}$ . (a) Case C121 with  $R_m = 1$ ,  $N = 10$ ; (b) Case C1230 with  $R_m = 30$ ,  $N = 10$ . The induced structural anisotropy is completely determined by the mean shear and is independent of the magnetic Reynolds.

stretch and align the turbulent eddies in the streamwise direction, strong rotation tends to induce columnar structures aligned with the rotation axis, while the action of the Lorentz force tends, through Joule dissipation, to promote long structures aligned with the mean magnetic field. Here, we examine eddy alignment under the combined action of  $S$ ,  $\Omega$  and  $B^{\text{ext}}$ . We first looked at a series of simulations in a fixed frame (zero frame rotation) in an effort to establish the effects of the simultaneous action of the mean shear and the spanwise magnetic field on the turbulence structure. Then we look at these effects in a spanwise rotating frame.

The diagnostic tool used to determine eddy alignment is the structure dimensionality tensor (Kassinis, Reynolds & Rogers, 2001), which for homogeneous turbulence is defined by

$$D_{ij} = \int E(k) \frac{k_i k_j}{k^2} d^3 \mathbf{k} \quad d_{ij} = D_{ij}/D_{kk} \quad D_{kk} = q^2 = 2k. \quad (5.1)$$

Note that each diagonal component of  $d_{ij}$  can attain values only between 0 and 1, and that for turbulence in which the energy-containing structures are elongated in the  $x_\alpha$  direction,  $d_{\alpha\alpha} \rightarrow 0$ . On the other hand  $d_{\alpha\alpha} \rightarrow 1$  corresponds to structures that are narrow and have strong gradients in the  $x_\alpha$  direction.

Figure 3 shows the evolution of the structure dimensionality when  $M = \tau_{\text{shear}}/t_m = 0.1$ . Two different values of the magnetic Reynolds number ( $R_m = 1$  and  $R_m = 30$ ) are considered. In both cases, the magnetic interaction number is  $N = 10$ . The evolution of the dimensionality anisotropy is dominated by the mean shear and is independent of the  $R_m$ . At large times,  $d_{11} \approx 0$ , indicating a predominance of long streamwise eddies.

The evolution of the dimensionality anisotropy for  $M = 20$  is shown in Figure 4. As expected, in this case the external spanwise magnetic field has a strong influence on the development of structure anisotropy. In the case when  $R_m = 1$ , the turbulence is driven towards a two-dimensional (2D) state corresponding to almost axisymmetric structures aligned with the direction of the magnetic field. Note however that when  $R_m = 30$ , the magnetic field is less effective in imposing the spanwise eddy alignment. In

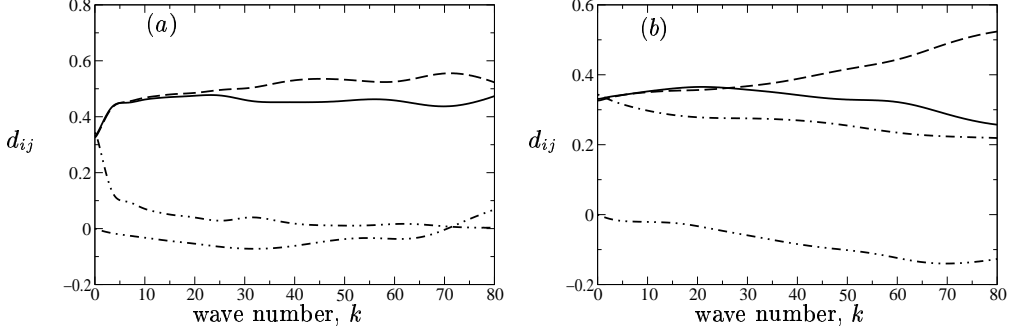


FIGURE 4. Evolution of the normalized dimensionality tensor in homogeneous MHD turbulence being sheared in a fixed frame ( $\lambda = 0$ ) with  $M = \tau_{\text{shear}}/\tau_m = 20$ : —  $d_{11}$ ; - - -  $d_{22}$ ; - · -  $d_{33}$ ; · · ·  $d_{12}$ . (a) Case C321 with  $R_m = 1$ ,  $N = 10$ ; (b) Case C3230 with  $R_m = 30$ ,  $N = 10$ . At low magnetic Reynolds numbers (on the left) the eddies are aligned with the external magnetic field in the spanwise direction. However, at moderately high magnetic Reynolds numbers (on the right) the mean shear is able to induce partial streamwise alignment.

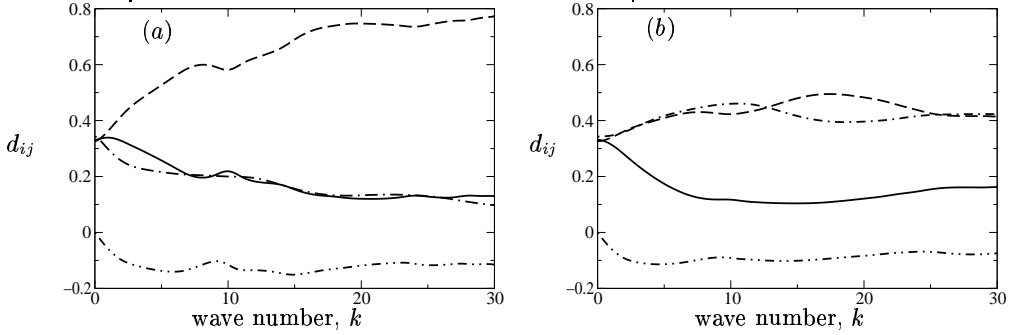


FIGURE 5. Evolution of the normalized dimensionality tensor in homogeneous MHD turbulence being sheared in a fixed frame ( $\lambda = 0$ ) with  $M = \tau_{\text{shear}}/t_m = 2$ : —  $d_{11}$ ; - - -  $d_{22}$ ; - · -  $d_{33}$ ; · · ·  $d_{12}$ . (a) Case C221 with  $R_m = 1$ ,  $N = 10$  (b) Case C2230 with  $R_m = 30$ ,  $N = 10$ . At low  $R_m$  (on the left) the turbulence structure is characterized by equal elongation in the streamwise and spanwise direction (corresponding to the horizontal sheets of Figure 7a). Thus the magnetic field and the mean shear are equally effective in inducing structural anisotropy. When  $R_m = 30$  (on the right), the mean shear dominates and the turbulence is characterized by long streamwise eddies.

fact, at this moderately high  $R_m$  the overall dimensionality anisotropy is suppressed as compared to the  $R_m = 1$  case. There is also evidence that at large times the mean shear is contributing more effectively in the anisotropy development, and as a result  $d_{11}$  and  $d_{33}$  seem to decrease at the approximately the same rate. This suggests that initially the structures become elongated in the spanwise direction under the action of the magnetic field. However, as the structures elongate the Joule dissipation becomes less effective, and this allows the shear to induce a streamwise elongation.

A more interesting anisotropy evolution is obtained in the case when  $M = 2$ , that is when the mean shear time scale is comparable to the Joule time. Figure 5a shows the

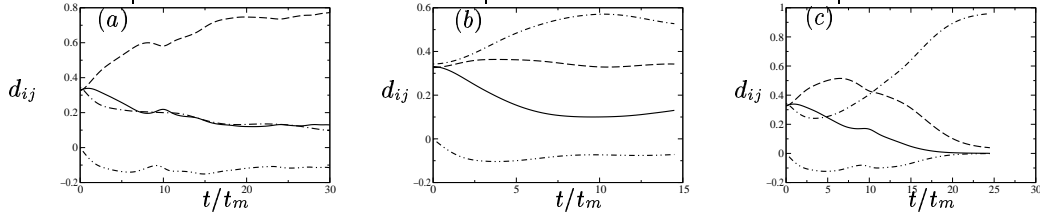


FIGURE 6. Evolution of the normalized dimensionality tensor in homogeneous MHD turbulence being sheared in a rotating frame with  $M = \tau_{\text{shear}}/t_m = 2$ : —  $d_{11}$ ; ----  $d_{22}$ ; -·-·  $d_{33}$ ; ····  $d_{12}$ . (a) Case C221 with  $R_m = 1$ ,  $N = 10$ , and  $\lambda = 0$  (no rotation); (b) Case C221 with  $B = 0$  and  $\lambda = 0.25$  (hydrodynamic case); (c) Case C221 with  $R_m = 1$ ,  $N = 10$ , and  $\lambda = 0.25$ . In a fixed frame and at low  $R_m$  (on the left) the turbulence structure is equally elongated in the streamwise and spanwise direction (corresponding to the horizontal sheets of Figure 7a). In the case of hydrodynamic ( $B = 0$ ) shear in a rotating frame (in the middle) there is preferential alignment of the turbulence eddies with the streamwise direction. When the magnetic field and the frame rotation act simultaneously (on the right), a bifurcation is observed where the structure transitions from a tendency towards horizontal sheets at short times, to vertical sheets at large times (see Figure 7c).

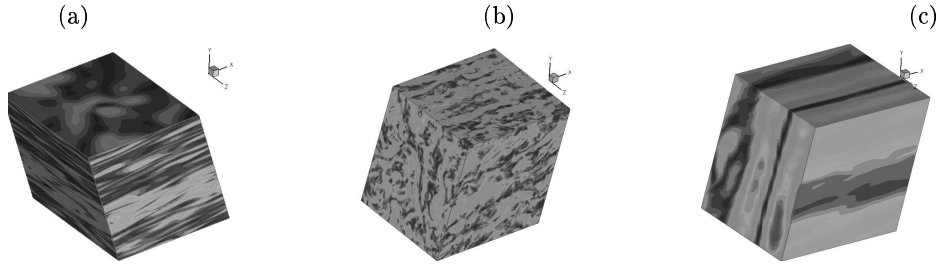


FIGURE 7. Velocity magnitude contours showing the structural anisotropy induced at large times by the combined action of spanwise frame rotation and spanwise mean magnetic field: (a) Case C221 ( $M = 2$ ,  $N = 10$ ,  $R_m = 1$ ) with zero frame rotation. The structure is characterized by horizontal slabs (equal elongation in the streamwise and spanwise direction); (b) Case C221 with frame rotation rate  $\lambda = 0.25$  and zero magnetic field (hydrodynamic case). Structures are mostly elongated and aligned with the streamwise direction. Some elongation is observed in the flow normal direction within the plane of the mean shear; (c) Case C221 with both the frame rotation ( $\lambda = 0.25$ ) and the magnetic field being active. The structure is characterized by vertical slabs.

evolution of the dimensionality anisotropy when  $R_m = 1$ . In this case,  $d_{11} \approx d_{33} \rightarrow 0$  suggesting that the mean shear and the external field are equally effective in inducing structural anisotropy. As result, at large times the turbulence is characterized by thin ( $d_{22} \rightarrow 1$ ) horizontal sheets. However, when  $R_m = 30$  (Fig. 5b) the mean shear dominates, inducing long, roughly axisymmetric, eddies aligned with the streamwise direction ( $d_{11} \rightarrow 0$ ).

So far we have considered the evolution of structure anisotropy in a fixed frame. Figure 6 shows the development of the normalized dimensionality tensor in the rotating frame for the case  $M = 2$ ,  $N = 10$ , and at  $R_m = 1$ . Figure 6a corresponds to 5a and shows that in the fixed frame, the magnetic field and the mean shear are equally effective in inducing two-dimensionality, and as a result the structure evolves towards a

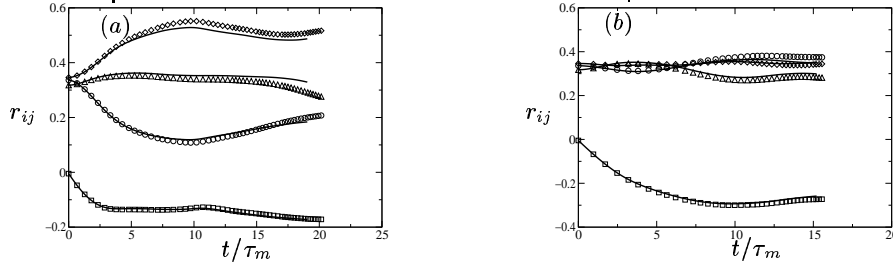


FIGURE 8. Comparison of the predictions of the Quasi-Linear approximation with those of full MHD for the evolution of the Reynolds stress components normalized by the tensor trace. Solid lines are the predictions of the DNS using the QL approximation, and symbols are DNS results for full MHD;  $\circ$   $r_{11}$ ,  $\square$   $r_{12}$ ,  $\diamond$   $r_{22}$ ,  $\Delta$   $r_{33}$ . (a)  $R_m = 50$ ,  $N = 10$ ,  $M = 2$ ,  $\lambda = 0.75$  and (b)  $R_m = 50$ ,  $N = 10$ ,  $M = 2$ ,  $\lambda = 0.25$

state characterized by horizontal sheets (see also Fig. 7a). In a frame rotating about the spanwise axis at a rate  $\lambda = 0.25$ , and in the absence of an external magnetic field (hydrodynamic case), the structure evolves towards a state characterized by elongated streamwise eddies ( $d_{11} \rightarrow 0$ ), as shown in Fig. 6. Note however, that these eddies tend to be somewhat elongated in the  $x_2$  direction, that is in the flow-normal direction within the frame of the mean shear ( $d_{22} < d_{33}$ ). This flattening of the eddies is also evident in the structure visualization of Fig. 7b. An interesting bifurcation seems to take place in the case when the frame rotation and the external magnetic field act concurrently (Fig. 6c). At short times, the evolution of the normalized dimensionality tensor is similar to the one obtained in the non-rotating case, and reveals a balance between the effects of the mean shear and the external magnetic field. At larger times, however ( $\tau/\tau_m \gtrsim 5$ ) a sudden transition takes place leading eventually to a state characterized by vertical slabs ( $d_{11} \approx d_{22} \rightarrow 0$  and  $d_{33} \rightarrow 1$ ). This effect has also been observed in cases C225 and C2210.

### 5.2. Validity of the Quasi-Linear Approximation

One of the questions that we wanted to answer concerns the range of validity of the Quasi-Linear (QL) approximation (3.7) and (3.8) in the presence of frame rotation and mean shear. Here, we recall that the QL approximation was originally proposed in the context of initially isotropic MHD turbulence (no mean deformation).

We have found that the QL approximation remains in excellent agreement with the full MHD predictions for all the magnetic Reynolds numbers that we have considered, which cover the range  $1 \leq R_M \leq 50$ . For example, Figure 5.2 shows the evolution of the components of the Reynolds stress tensor normalized by the tensor trace. The predictions of the QL approximation are shown as solid lines and those of the full MHD are shown as symbols. Two different values of  $\lambda$  are considered, and in both cases the QL and the full MHD predictions are in excellent agreement even though the magnetic Reynolds number is relatively high ( $R_m = 50$ ).

### 5.3. Augmentation of Turbulence in the Counter-Rotating Case

One of the main aims of this work was to establish the effect that the combined action of an external magnetic field, mean shear, and frame rotation can have on the stability of MHD turbulence.

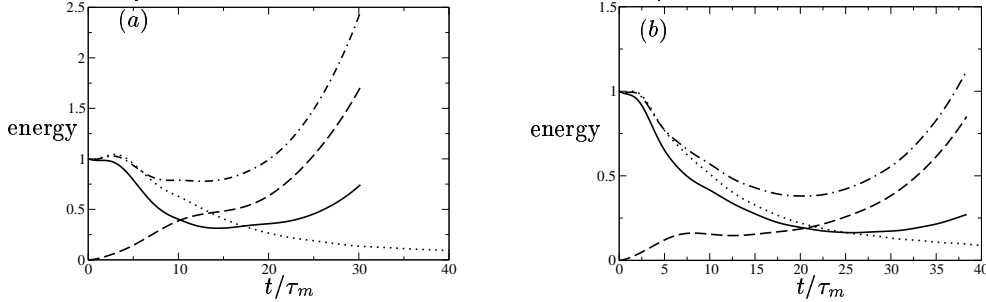


FIGURE 9. Augmentation of shear turbulence in a rotating frame by the imposition of a spanwise magnetic field for the case  $R_m = 50$ ,  $N = 10$ ,  $M = 2$ : ——— turbulent kinetic energy normalized by its initial value  $k/k_0$ ; - - - - magnetic energy normalized by initial turbulent kinetic energy  $E_b/k_0$ ; - · - · - total energy normalized by initial turbulent kinetic energy  $(k + E_b)/k_0$ ; ····· turbulent kinetic energy for the hydrodynamic ( $B = 0$ ) case. (a)  $\lambda = 0.75$ , and (b)  $\lambda = 1.0$ .

For the hydrodynamic case, it is well known that frame rotation can act to either suppress or augment turbulence. The parameter that determines which of the two happens is the ratio of the frame rotation rate to the mean shear rate  $\lambda = \Omega^f/S$  (see Figure 2). For moderate counter-rotation of the frame relative to the intrinsic shear rotation, ( $-0.1 \lesssim \lambda \lesssim 0.51$ ), the turbulence is augmented as a result of the frame rotation. This is often referred to as the “unstable” regime.

Even though we are still analyzing some of the cases that were simulated during the summer program, we have identified several cases where the presence of the external magnetic field, combined with the rotation of the frame and the mean shear, leads to expansion of the “unstable” regime. We have also identified conditions under which the magnetic fields seems to have little if any effect on the stability of the rotating shear flow.

All the cases where the magnetic field was found to lead to augmentation of the turbulence lie on the left of the bifurcation envelope. That is they correspond to cases where the frame counter rotates at a rate that is equal or larger than the rotation rate associated with the mean shear (see Figure 2). In all cases the external magnetic field was in the spanwise direction. On the contrary, preliminary results of cases involving a streamwise external magnetic field and spanwise frame rotation failed to show a strong effect on the stability of turbulent shear flow.

The effect of an imposed spawise magnetic field on the time histories of the turbulent magnetic and kinetic energies is shown in Figure 9 for two different values of  $\lambda$ . Both values of  $\lambda$  are high enough, that in the hydrodynamic case a suppression of the turbulence is observed as evidenced both by the decay of  $k$  in time, and also by the fact that  $P/\epsilon < 1$ . In the magnetohydrodynamic cases, after an initial transient, both the turbulent kinetic energy  $k$  and the turbulent magnetic energy  $E_b$  grow exponentially in time. In fact, at larger times, the magnetic energy exceeds the kinetic energy:  $E_b > k$ .

The evolution of the ratio of the production of the turbulent kinetic energy to its dissipation rate is shown in Figure 10. In the hydrodynamic case,  $P/\epsilon < 1$  at large times indicating that the turbulence is suppressed a result of the strong counter-rotation of the frame. However, when the spanwise magnetic field is present,  $P/\epsilon > 1$  at large times, indicating that the turbulent kinetic energy is augmented as a result of the combined effects of the  $\Omega^f$  and  $B$ .

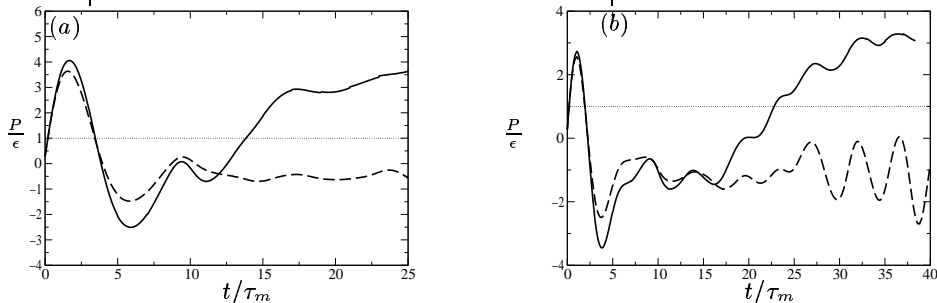


FIGURE 10. Augmentation of shear turbulence in a rotating frame by the imposition of a spanwise magnetic field for the case  $R_m = 50$ ,  $N = 10$ ,  $M = 2$ : — production over dissipation ( $P/\epsilon$ ) for the MHD case; ---- production over dissipation ( $P/\epsilon$ ) for the hydrodynamic ( $B = 0$ ) case; (a)  $\lambda = 0.75$ , and (b)  $\lambda = 1.0$ .

#### 5.4. Scale Dependence of Anisotropy

The scale dependence of anisotropy in incompressible MHD turbulence at moderate magnetic Reynolds numbers remains an open question. For compressible turbulence at high magnetic Reynolds numbers, Cho and Lazarian (2003) have found that Alfvén mode velocity fluctuations show a strong scale dependence, with the small scales being more anisotropic than the larger ones.

We have attempted to obtain a scale dependent measure of anisotropy using the spectra of the turbulence structure dimensionality tensor (Kassinis, Reynolds & Rogers, 2001). Thus we define

$$d_{ij}(k) = \sum_{\text{shell}} E(k) \frac{k_i k_j}{k^2} / \sum_{\text{shell}} E(k) \quad d_{ii}(k) = 1, \quad (5.2)$$

where the summation in (5.2) is over shells in Fourier space. For turbulence that is isotropic at the scale set by  $k$  we have  $d_{ij}(k) = \delta_{ij}/3$ . For turbulence that it is two-dimensional (2D) independent of direction  $x_\alpha$ ,  $d_{\alpha\alpha}(k) = 0$ .

Figure 11 shows the anisotropy levels obtained for two cases with frame rotation (C2250 with  $\lambda = 0.75$  and C2250 with  $\lambda = 1.0$ ). Variations at very low wavenumbers are spurious and attributed to limited sample. On the other end of the spectrum, variations beyond  $k \approx 128$  are again contaminated by the progressive loss of modes that extend beyond the limits of the computational box (for these  $256^3$  simulations). In the intermediate range that lies between these limits, anisotropy as measured by  $d_{ij}(k)$  seems to exhibit a weak increase with wave number, especially in the flow-normal directions. This trend is suggestive of the observations of Cho and Lazarian (2003) in compressible MHD turbulence at high  $R_m$ . Cases with low  $R_m$  did not seem to exhibit this increase of anisotropy with decreasing scale, but a more careful analysis for our results is needed in order to establish a possible Reynolds number dependence. Both cases correspond to  $M = 2$ , that is the time scale associated with the mean shear is twice as large as the time scale associated with the diffusion of the magnetic field. Yet, in both cases,  $d_{11}(k) \approx 0$  for the entire range of wave numbers over which results are meaningful. Thus at these relatively high  $R_m$ , the mean shear seems to determine the overall structural anisotropy when the two time scales are comparable. Because of the limited size of the computational box, we were unable to adequately answer the question of anisotropy at small scales. We plan to carry

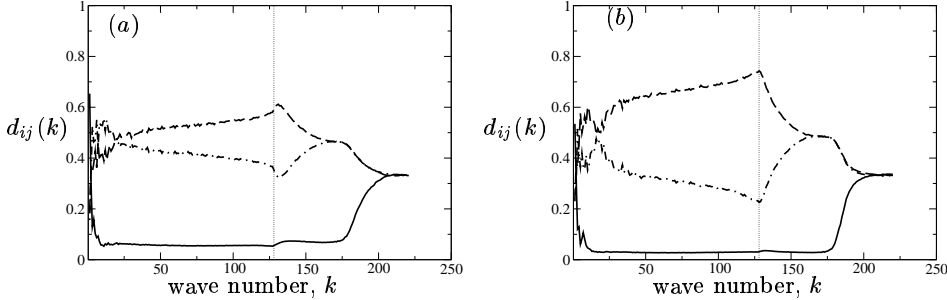


FIGURE 11. Scale dependence of anisotropy as measured by  $d_{ij}(k)$  (see 5.2) in homogeneous MHD turbulence being sheared in a rotating frame: —  $d_{11}(k)$ ; - - -  $d_{22}(k)$ ; - · -  $d_{33}(k)$ . (a) Case C2250 ( $R_m = 50$ ,  $N = 10$ ,  $M = 2$ ) with  $\lambda = 0.75$  and  $t/t_m = 31.7$ , and (b) Case C2250 ( $R_m = 50$ ,  $N = 10$ ,  $M = 2$ ) with  $\lambda = 1.0$  and  $t/t_m = 38.0$ .

a series of  $512^3$  simulations in order to address that question more thoroughly. We also hope that these higher-resolution simulations will allow us to clarify the slight increase of anisotropy that was observed in the cases discussed above.

## 6. Conclusions and future plans

We have used direct numerical simulations to examine the dynamics of homogeneous MHD turbulence subjected to mean shear in fixed and rotating frames. We have found that the most interesting dynamics is observed when the time scale of the mean shear is comparable to that of the applied magnetic field. In this regime, the magnetic field and the mean shear exert competing influences on the structure of the turbulence and relatively small variations in the governing parameters seem to lead to markedly different evolving states.

One particularly significant result concerns the combined effects of the mean magnetic field and the frame rotation on the evolution of the turbulent kinetic energy. We have found that at sufficiently high magnetic Reynolds numbers,  $R_m \gtrsim 40$ , the application of a spanwise magnetic field leads to augmentation of the turbulence even for cases where in absence of the magnetic field the turbulence is suppressed as a result of the frame rotation. We have observed this effect for cases where the frame is counter-rotating relative to the intrinsic rotation associated with the shear, and for values of the ratio of the frame rotation rate to the shear rate beyond  $\eta \approx 0.51$ , the limit which marks the onset of suppression of the turbulence as  $\eta$  is increased. In these flows, it was found that the magnetic field energy, which initially is zero, grows and quickly surpasses the turbulent kinetic energy. No such augmentation of the turbulence was observed for cases where the frame is co-rotating with the shear. Preliminary runs where the magnetic field was aligned with the streamwise direction also failed to exhibit such a strong augmentation of the turbulence as a result of the presence of the field.

We have also examined the range of validity of the Quasi-Linear (QL) approximation that was introduced by Kassinos *et al.* in the 2002 CTR Summer Program. The QL approximation was originally evaluated only in the absence of mean deformation. We have found that the predictions of the QL approximation were in excellent agreement with those of the full MHD, for all the magnetic Reynolds numbers we have considered

(up to  $R_m = 50$ ). Other dimensionless parameters, such as the ratio of the shear time scale to the time scale for magnetic diffusion, seem to have little effect on the validity of the approximation.

During the summer program we have generated a substantial amount of data. In the coming months, we plan to analyze this more carefully in order to identify mechanisms and effects that we want to examine more closely. To understand such effects we plan a series of higher resolution runs. We hope this work will lead to an improved fundamental understanding of the combined effects of mean shear, frame rotation and magnetic fields on MHD turbulence. We plan to use this understanding for the development of improved structure-based models of MHD shear turbulence. A deeper understanding of the mechanisms that lead to instability and anisotropy in these flows is also important in the study of accretion in stellar disks and in engineering applications such as magnetogasdynamics.

#### REFERENCES

- CHO, J. & LAZARIAN, A. 2003 Compressible magnetohydrodynamic turbulence: mode coupling scaling relations, anisotropy, viscosity-damped regime and astrophysical implications. *Monthly Not. Royal Astron. Soc.*, **345**, 325-339.
- KASSINOS, S. C. & REYNOLDS, W. C. 1999 Structure-based modeling for homogeneous MHD turbulence. *Annual Research Briefs*, Center for Turbulence Research, NASA Ames/Stanford Univ., 301-315.
- KASSINOS, S. C., KNAEPEN, B. & CARATI, D. MHD turbulence at moderate magnetic Reynolds number. Proceedings for the 2002 Summer Program, Center of Turbulence Research, Stanford/NASA Ames.
- KASSINOS, S.C. REYNOLDS, W.C. & M. M. ROGERS 2001 One-point turbulence structure tensors. *J. Fluid Mech.*, 428, 213-248.
- KASSINOS, S. C. & REYNOLDS, W. C. DNS and Structure-Based Modeling of Rotated Homogeneous Shear Flows. Proceedings of the *Third International Symposium on Turbulence and Shear Flow Phenomena*, Sandai, Japan, June 2003.
- KNAEPEN, B., KASSINOS, S.C., & CARATI, D. 2004 MHD turbulence at moderate magnetic Reynolds number. *J. Fluid Mech.*, (in press).
- MOFFATT, H.K. 1967 On the suppression of turbulence by a uniform magnetic field. *J. Fluid Mech.* **28**, 571-592.
- ROBERTS, P. H. 1967 *An Introduction to Magnetohydrodynamics*. Elsevier, New York.
- ROGALLO, R.S. 1981 Numerical experiments in homogeneous turbulence.